Radiative-Gasdynamic Coupling and Nonequilibrium Effects behind Reflected Shock Waves

LELAND A. CARLSON*
Texas A&M University, College Station, Texas

Results of calculations for the flowfields behind reflected shock waves in nitrogen resulting from incident shock velocities of 8 and 11 km/sec and initial pressures of 10^{-3} and 10^{-2} cm of Hg are presented. In obtaining these results the radiative properties of the gas have been represented by an approximate nongray absorption coefficient model, and the exchange of momentum and energy due to collisions between particles has been included. During the first microsecond after reflection the radiative cooling is strong enough to cause the end-wall pressure to decrease as much as 50% before increasing to its equilibrium value. The cooling also induces a velocity acceleration towards the wall and accelerates chemical and thermal relaxation. In the region immediately behind the shock wave the electron temperature is much lower than the heavy particle temperature, but even in the near equilibrium region next to the wall the electron temperature remains about two percent below the heavy particle temperature. Comparison calculations demonstrate that two temperature effects must be included to accurately predict end-wall pressure, radiative heat transfer, and radiative-gasdynamic coupling effects.

Introduction

At very high re-entry velocities, the equilibrium temperature in the bow shock region of an entry vehicle can reach 20,000°; and the heat transfer to the vehicle and the flowfield around it will be dominated by thermal radiation. As a consequence for the past several years reflected shock waves have been used to study high-temperature and radiative-gasdynamic phenomena typical of re-entry.

Previous reflected shock studies,[1,2] however, consider conditions which, while of definite interest, do not represent the nonequilibrium phenomena associated with very high altitude, high-velocity re-entry. At the low pressures corresponding to conditions of interest in atmospheric entry there are portions of the reflected shock flowfield in which chemical nonequilibrium effects can be significant.[3] For example, in the region immediately behind a reflected shock front large gradients in temperature and species concentration can occur; and such variations can affect the radiative heat transfer through changes in the concentration and temperature of the radiating species.

Besides chemical nonequilibrium, it is possible for a partially ionized gas to have regions of thermal nonequilibrium between electrons and the other heavier species. This type of nonequilibrium results because the rate of energy exchange between electrons and heavy particles is very slow due to large mass differences in the species, and it is characterized by different electron and heavy body temperatures. Thermal nonequilibrium of this nature has been predicted[4] and indirectly observed[5] in the region behind a shock front. Since radiation is primarily governed by the electron temperature, thermal nonequilibrium might have a significant effect on the nature and magnitude of the radiative-gasdynamic coupling and the end-wall radiative heat transfer. In addition, many reflected shock-wave experimental measurements are time integrated, and any significant nonequilibrium effects at short times could affect the interpretation of such results.

Since at low densities chemical and thermal nonequilibrium effects may be important and may strongly affect such quantities as the radiative heat transfer, further investigation of these phenomena for the case of the reflected shock wave would be valuable. Thus, the present study has been initiated with the primary purposes of 1) developing a solution to the radiating reflected shock problem including chemical nonequilibrium and two temperature effects, and 2) investigating the extent and interaction of two-temperature, chemical nonequilibrium, and radiative-gasdynamic coupling effects behind high enthalpy reflected shock waves.

Formulation of the Problem

In a cylindrical shock-tube the reflected shock-wave problem is a two-dimensional unsteady problem in x and r. However, in the vicinity of the shock-tube centerline, the flow is essentially one-dimensional in x; and, thus, in the interest of simplification the present problem is treated as one-dimensional. This approach not only serves to simplify the equations but also makes the integrals in the radiation terms easier to evaluate. The distance x is measured from the end-wall; and the time t is counted from the instant of shock reflection. All of the fluid dynamic properties between the shock wave and the end-wall are considered functions of distance and time, and the velocity of the reflected shock front is assumed to be a function of time. This time dependence is necessary in order to account for any shock attenuation effects resulting from radiation cooling. The continuity and momentum equations that are used are as follows:

$$\partial\rho_i/\partial t + \partial(\rho_i u)/\partial x + \partial(\rho_i U_i)/\partial x = \dot{W}_1 \quad (1)$$

$$\partial\rho/\partial t + \partial(\rho u)/\partial x = 0 \quad (2)$$

$$\rho\partial u/\partial t + \rho u\partial u/\partial x = -\partial p/\partial x \quad (3)$$

Presented as Paper 70-774 at the AIAA 3rd Fluid and Plasma Dynamics Conference, Los Angeles, June 29–July 1, 1970; submitted August 17, 1970; revision received December 11, 1970. The formulation and 11 km/sec, 10 μ Hg results were performed while the author was a Research Associate at The Ohio State University. The author wishes to thank R. M. Nerem for his encouragement and advice and T. Benson for assisting with some of the calculations. This work was supported by NASA Grant NGR-36-008-106 to The Ohio State University. Partial support has been furnished by the Numerical Computation Laboratory of OSU and the Texas A&M University Research Council.

* Assistant Professor. Associate Member AIAA.

Since it is the aim of this study to investigate the reflected shock region including the effects of thermal nonequilibrium, there should in principle be an energy equation for each species. However, since the exchange of energy in elastic collisions is dependent upon the mass ratio of the colliding particles, it is assumed that for particles of almost the same mass the temperature equilibrates in a few collisions. Thus, the heavy particles (i.e., atoms, molecules, and ions) are all characterized by the same temperature T_H; but the electrons are permitted to have a different temperature T_e. Hence only two energy equations are needed. One is the electron species energy equation, which neglecting terms of order (m_e/m_a) is

$$\rho_e \frac{\partial h_e}{\partial t} + \rho_e u \frac{\partial h_e}{\partial x} + \frac{\partial}{\partial x}\left(-\lambda_e \frac{\partial T_e}{\partial x}\right) + \frac{\partial}{\partial x}(\rho_e U_e h_e) - \frac{\partial p_e}{\partial t} - u\frac{\partial p_e}{\partial x} + \dot{w}_e h_e - h_e \frac{\partial}{\partial x}(\rho_e U_e) - \dot{w}_e \frac{u^2}{2} = U_e \frac{\partial p_e}{\partial x} + \sum_{j=1}^{s} \xi_{ej} + U_e \sum_{j=1}^{s} P_{ej} + Q_e \quad (4)$$

The first term on the right-hand side represents the effect of external forces and is obtained from the electron momentum equation. The second term is the rate of energy gain by electrons due to elastic encounters because of thermal motion of the particles; while the third term accounts for the energy gain resulting from elastic collision because of the relative fluid motion of the electrons. The last term Q_e represents energy change due to inelastic encounters.

Analytic expressions for the terms ξ_{ij} and P_{ij} have been derived and are presented in Ref. 6. For example,

$$\xi_{ij} = \frac{(m_i m_j)^{5/2} N_j N_i S_{ij}}{(m_i + m_j)^2 (m_i T_j + m_j T_i)^{1/2} (2\pi)^{1/2} k^{3/2}} \left\{ \frac{m_i m_j (T_j - T_i)}{K \Delta U} \left[\left(\frac{\pi}{K}\right)^{1/2} \left(\frac{\Delta u^4}{4} + \frac{3\Delta U^2}{4K} + \frac{3}{16K^2} \right) \times 2\,\mathrm{erf}(K^{1/2}\Delta U) + 2\exp(-K\Delta U^2) \left(\frac{\Delta U^3}{4K} + \frac{5}{8}\frac{\Delta U}{K^5} \right) \right] + \frac{m_j T_i (m_i + m_j)}{2K^2 \Delta U} \left[\left(\frac{\pi}{K}\right)^{1/2} \mathrm{erf}\,(K^{1/2}\Delta U) \left(K\Delta U^4 + \Delta U^2 - \frac{1}{4K} \right) + \Delta U^3 \exp(-K\Delta U^2) + \frac{\Delta U}{2K} \exp(-K\Delta U) \right] \right\} \quad (5)$$

where $\Delta U = |\mathbf{U}_i - \mathbf{U}_j|$, $K = [2kT_i/m_i + 2kT_j/m_j]^{-1}$, and S_{ij} is the collision cross section.

For the second energy expression the global energy equation, Eq. (6), is used

$$\rho \frac{\partial h}{\partial t} + \rho u \frac{\partial h}{\partial x} + \frac{\partial}{\partial x}\left[\sum_{i=1}^{s} \left(-\lambda_i \frac{\partial T_i}{\partial x} \right) \right] + \frac{\partial}{\partial x}\left[\sum_{i=1}^{s} \rho_i U_i h_i \right] + \frac{\partial q_R}{\partial x} - \frac{\partial p}{\partial t} - u\frac{\partial p}{\partial x} = -\sum_{i=1}^{s} \dot{w}_i h_i^0 \quad (6)$$

The viscous stress terms are omitted in Eqs. (3, 4, and 6) because their expected effect in the reflected shock region is negligible. Also, a radiative heat-transfer term appears only in the global energy equation because it is assumed that the radiation effect on electron energy is negligible.

In the mathematical formulation, the enthalpy-temperature relationship is obtained by application of statistical mechanics and the appropriate partition functions. The electronic terms are formulated using the electron temperature, assuming that the electronic levels are in equilibrium with the free electrons.[4,7] The transport coefficients are derived from kinetic theory relationships, and the diffusion velocity expressions are based upon an ambipolar diffusion model. Both are suitably modified for mixture and two-temperature effects.

Nitrogen has been selected as the test gas because of its similarity at high temperatures to air. A set of chemical reactions and rate constants representative of high temperature nitrogen has been used and is presented in Table 1. The dissociation constants are from Ref. 3, and the ionization rates are based on the experimental results of Wilson.[7] Also, the mass production rate expressions for the ionization reactions assume that these reactions proceed via excitation of the nitrogen atom to the $3s^4P$ state and subsequent rapid ionization.[7]

The radiation term in the overall energy equation has been formulated, following the basic approach of Anderson,[1] for the case where the absorption coefficient is represented by a multistep model. Its resultant form is given by Eq. (7)

$$-\frac{\partial q_R}{\partial x} = -4\pi \sum_i \alpha_i B_i + 2\pi \sum_i \alpha_i \int_0^{\tau_{si}} B_i(z,t) E_1(\tau_i - z)\,dz \quad (7)$$

Here the summation is over the spectral regions of the step model, and α_i and B_i are the values of the absorption coefficient and integrated blackbody function for a given wavelength region. For the absorption coefficient the experimentally verified five-step nongray absorption coefficient model of Knott, Carlson, and Nerem[8] is used. This model is representative of high-temperature radiating nitrogen and includes infrared lines, the visible continuum, vacuum-ultraviolet lines, and the vacuum-ultra-violet continuum.

This investigation is the first study to include in a reflected shock flowfield solution the combined and interacting effects of chemical nonequilibrium and nongray radiative transfer. Also, it is the first nonequilibrium reflected shock formulation which permits the electrons to have a temperature different from the other species. Several solutions have been obtained using a computational technique based upon a forward-in-time finite-difference scheme similar to that of Ref. 1. Further details of the present formulation and solution of the radiating reflected shock problem are presented in Ref. 9.

Discussion of Results

In selecting the shock-tube conditions to be investigated, several items have to be considered. The equilibrium temperature behind the shock wave has to be sufficiently high that radiative processes and radiative transfer are significant, and the chemical relaxation time needs to be long enough that nonequilibrium effects can be observed. Conditions compatible with these requirements can be determined by

Table 1 Chemical reactions and reaction rate constants

Reaction	Rate
$N_2 + N_2 \rightleftarrows 2N + N_2$	$K_b = 1.5 \times 10^{20} T_H^{-1.5}$
$N_2 + N \rightleftarrows 2N + N$	$K_b = 7.5 \times 10^{20} T_H^{-1.5}$
$N_2 + M \rightleftarrows 2N + M$	$K_b = 1 \times 10^{19} T_H^{-1.5}$
$N + N^+ \rightleftarrows 2N^+ + e$	$K_f = 2.34 \times 10^{11} T_H^{1/2} e^{-120000/T_H}$
$N + e \rightleftarrows N^+ + 2e$	$K_f = 4.16 \times 10^{13} T_e^{1/2} [1 + T_e/60000]_e^{-120000/T_e}$
$N + N \rightleftarrows N^+ + e^- + N$	$K_f = 2.34 \times 10^{11} T_H^{1/2} e^{-120000/T_H}$

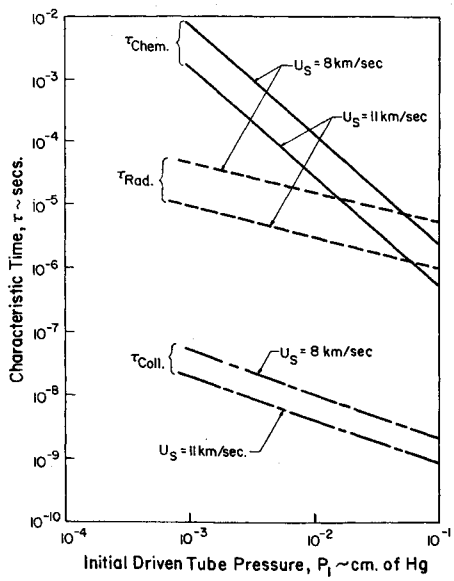

Fig. 1 Characteristic times behind reflected shock waves in nitrogen.

comparing characteristic times representative of the time required for complete radiative cooling, the time required for complete deionization, and the time required for thermal equilibration by collisions alone. Such comparisons are shown for two incident shock velocities on Fig. 1, and it can be seen that the characteristic chemical recombination times at the low pressures are quite long and significantly longer than those required for radiative cooling. In fact, these results indicate that immediately behind a reflected shock wave radiative cooling can occur simultaneously with and possibly prior to chemical relaxation.

To increase the possibility of observing such an early cooling effect, a reflected shock flowfield corresponding to an incident shock velocity of 11 km/sec and an initial pressure of 10^{-3} cm Hg has been selected as the primary calculation condition. Admittedly, the shock front is thick for such a condition, but as can be seen in Fig. 1 a lower initial pressure offers a greater probability of observing the radiative cooling—chemical relaxation interaction. In addition, if these 10^{-3} cm Hg results show no significant effects due to chemical and thermal nonequilibrium, then such effects can be assumed to be negligible at higher pressures of say 10^{-2} cm Hg, where the shock front is by comparison thin. If they show important effects, then the direction for future calculations will be indicated. It should be noted that results have also been

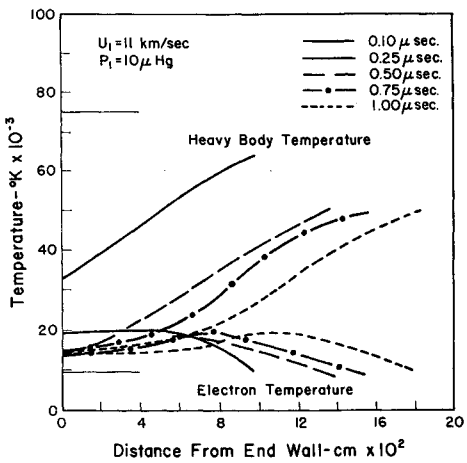

Fig. 2 Electron and heavy particle temperature profiles behind a reflected shock wave in nitrogen.

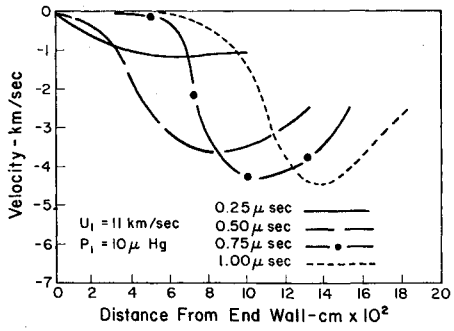

Fig. 3 Velocity profiles behind a reflected shock wave in nitrogen.

obtained for incident shock velocities of 8 and 11 km/sec at an initial pressure of 10^{-2} cm Hg. In all cases, convergence has been verified by changing the step size and comparing the results.

Figure 2 shows typical results for electron and heavy particle temperatures. Precursor effects are ignored for these calculations, and the gas in front of the reflected wave is considered to be in equilibrium. Initially the postshock heavy particle temperature is 75,000°K while that of the electrons is 9300°K. However, collisions between the electrons and the heavy particles cause the electron temperature to increase rapidly, and by 0.25 μsec the electron temperature over a large part of the flowfield has stabilized at about 19,500 °K. This stabilization or pseudoequilibrium of the electron temperature is caused by a balance between collision effects, which tend to increase the electron temperature, and ionization effects, which tend to decrease it. The gas radiates strongly at such high electron temperatures, and as a result by 0.25 μsec the heavy body temperature has cooled to almost 30,000°K. In fact, this decrease is mostly due to radiation cooling since at 0.25 μsec the dominating term in the energy equation is the radiation term. At this short time the ionization effects, while significant, are still small in comparison to the radiation effects.

By 0.50 μsec the temperature profiles are characteristic of flows in thermal nonequilibrium.[4,5] The heavy body temperature behind the shock front has decreased, due to shock-wave attenuation, to about 49,000°K; and at the wall the gas has cooled to about 14,000°K. The electron temperature increases as before from its low value behind the shock wave to about 19,500°K. By this time, however, electron-atom ionization processes, which tend to decrease electron energy and temperature, dominate; and the electron temperature decreases as the wall is approached. A similar analysis and explanation applies to the profiles at 0.75 μsec and 1.00 μsec except that more of the flowfield is characterized by temperatures below 20,000°K. Clearly, even at 1.00 μsec over two-thirds of the flowfield is characterized by extensive thermal nonequilibrium.

One interesting feature which is observable in Fig. 2 is that the electron temperature does not change very much in comparison to the heavy body temperature. Over most of the flowfield it is very close to the reflected shock equilibrium temperature. Thus, in future calculations it might be a suitable simplifying approximation to assume that the electron temperature has a constant value equal to the equilibrium temperature. It should be also noted that this essentially constant behavior of the electron temperature partially explains why low density stagnation point radiative heat-transfer shock-tube data[10] can be interpreted using equilibrium properties. As can be seen from Fig. 2, however, such interpretation is strictly fortuitous since such flows should have significant nonequilibrium regions.

The flow velocity between the shock wave and the wall is presented in Fig. 3 and due to nonequilibrium and radiative

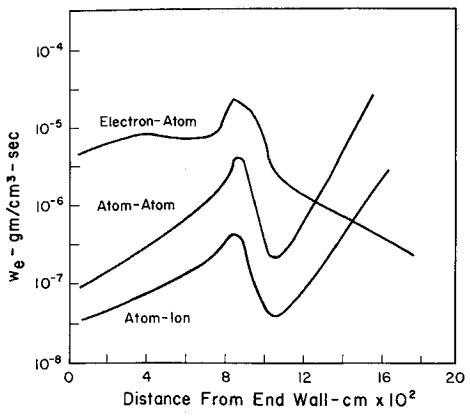

Fig. 4 Comparison of electron production rates at 1.00 μsec.

cooling it is not zero. Notice that in contrast to a nonradiating reflected shock flow, the magnitude of the velocity increases from its value behind the shock before beginning its decrease to the wall value. This initial acceleration results because in the immediate post-shock region cooling occurs sufficiently rapidly and without a corresponding density increase so that there is an initial pressure decrease. Since velocity is very sensitive to any pressure gradient, such a pressure decrease creates an acceleration towards the wall.

Understanding of the chemical nonequilibrium phenomena can be obtained by comparison of the chemical production rates of electrons as portrayed on Fig. 4. Obviously, the atom-atom reaction is predominant behind the shock front, and the electron-atom reaction predominates near the wall. Between the shock and the wall, however, the production rates are dependent not only upon the concentrations of the colliding partners but also upon the electron and heavy particle temperatures. Since in the region immediately behind the shock the concentrations are relatively constant and the heavy body temperature is decreasing rapidly, a decrease in the atom-atom and atom-ion production rates would be expected. On the other hand the only temperature affecting the atom-electron production rate is the electron temperature. Thus, in the immediate past-shock region the initial increase in the electron temperature causes the indicated rise in the electron-atom rate.

By 0.10 cm the free electron population has increased enough and the electron temperature is sufficiently high so that electron avalanche occurs. Due to the fact that one of the collision partners in the electron-atom reaction is an electron, the ionization rate avalanches or increases exponentially with the electron concentration until recombination begins to compensate appreciably for ionization.[11] Thus, the maximum value of the electron-atom rate at about 0.09 cm marks the point where collisional recombination becomes more important than collisional ionization. After the peak, the rate tends to decrease but at a slow pace because the

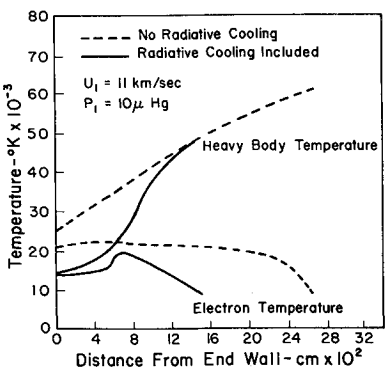

Fig. 5 Comparison of temperature profiles at 0.75 μsec with and without radiative cooling.

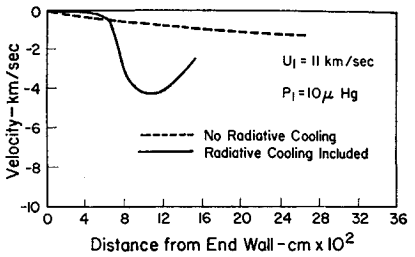

Fig. 6 Comparison of velocity profiles at 0.75 μsec with and without radiative cooling.

electron density is increasing in this region while the electron temperature is decreasing slowly. Also, as shown by other investigators,[4,5,7,12] the mixture density increases sharply at the beginning of the recombination zone.

Notice in Fig. 4 that nowhere is the atom-ion electron production rate ever significant. Thus future calculations might be simplified by ignoring the atom-ion chemical reaction completely. Also the variation of the atom-electron ionization rate and its dominance everywhere but immediately behind the shock is in agreement with the incident shock results of Petschek and Byron[12] in argon and Wilson[7] in nitrogen. This agreement and lack of dominance of the electron-atom rate immediately behind the shock might seem surprising in view of the large number of electrons in the region due to incident shock ionization. The explanation is that the initially low value of the electron temperature retards the atom-electron ionization rate until later in the relaxation zone.

The most significant result, however, of the present investigation is the existence of strong radiative gasdynamic coupling at short times after reflection. Even though for these conditions the absorption coefficient in the vacuum-ultraviolet is very large, the shock layer is so thin that the gas is essentially transparent and very strongly radiating. Figures 5–7 show comparison calculations which respectively include and exclude radiative cooling effects. In the latter case, which is called the no radiative cooling case in the figures, the radiative transfer term is deleted from the energy equation. By comparing the two sets of results, the effect and magnitude of radiative energy transfer can be determined. Figure 5 compares the temperature profiles for the two cases for a time of 0.75 μsec after reflection. In the radiative cooling case, both the electron and heavy particle temperatures near the wall have values below 20,000°K; but the noncooled calculation exhibits heavy body temperatures greater than 25,000°K and electron temperatures around 22,000°K. In addition, the cooled results indicate that at the wall thermal equilibration essentially exists for times longer than 0.45 μsec. However, in the radiation uncoupled case the wall heavy particle and electron temperatures are still over 4000°K apart at 0.75 μsec. Furthermore, the radiative cooling results indicate that the local equilibrium temperature is about 14,000°K and that near the wall such a temperature is achieved approximately 0.70 μsec after reflection. The uncoupled results show a temperature 10,000° K higher at 0.75 μsec. Finally, the shock position for the two calculations differs by about a factor of two.

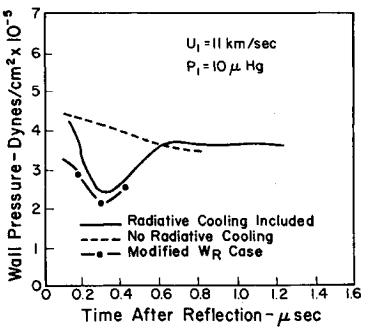

Fig. 7 Comparison of the variation of wall pressure with and without radiative cooling.

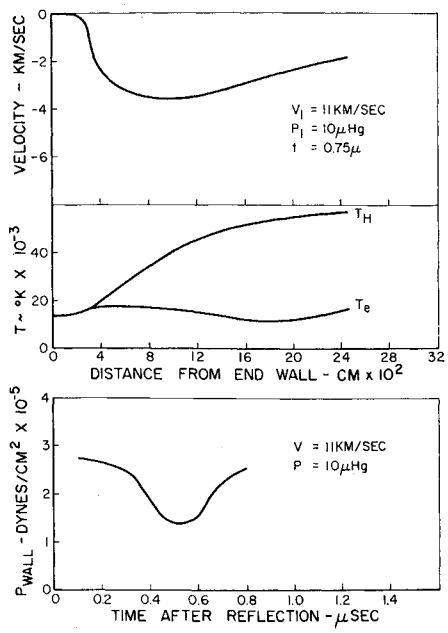

Fig. 8 End-wall pressure, temperature, and velocity profiles behind a reflected shock wave—frozen incident shock flowfield case.

Since the only difference in the two computations is the inclusion of radiative cooling, it can be deduced that even at short times after reflection radiative transfer has a pronounced cooling effect. More importantly, however, radiative transfer affects the relaxation zone by shortening the time and distance for both chemical and thermal relaxation and by inducing strong shock wave attenuation. Thus, it would appear that in order to obtain accurate results for even short times radiative cooling cannot be ignored.

Further evidence of radiative transfer effects in the relaxation zone appear in the cooled and uncooled velocity profiles of Fig. 6. In the no radiative cooling case, there is no evidence whatsoever of the velocity acceleration towards the wall that is so prevalent in the complete calculations. Thus, this velocity pattern, which results directly from the pressure variation, is an indirect manifestation of the radiative cooling effects that must be included in order to obtain valid results. It should be noted that while previous results have shown radiation coupling effects in the equilibrium zone behind reflected shock waves,[1] it is believed that these results are the first to show the existence of strong radiative-gasdynamic coupling effects in the actual relaxation zone behind the shock front. Furthermore, similar radiative-gasdynamic effects might occur in the thin shock layers surrounding small models located in low-density shock-tube flows.[10]

The variation in end-wall pressure is presented in Fig. 7, and the result for the cooled case also reflects the effects of radiative transfer. From its initially relatively high value corresponding to frozen flow conditions, the end-wall pressure decreases to a minimum value at about 0.35 μsec and then increases. At about 0.70 μsec it attains a value which remains relatively constant for the rest of the calculation and which is almost identical to the ideal equilibrium value of 3.6×10^5 dynes/cm². Obviously this rather marked initial decrease in pressure of almost a factor of two must be due entirely to the effects of radiative cooling since in the uncoupled case the wall pressure decreases slowly and steadily from its frozen value without the dip evident in the complete calculation. The explanation is that as the gas cools due to radiation, the accompanying change in number density is small because chemical effects have not yet had time to become important. Thus the pressure must decrease.

In order to ascertain whether or not end-wall thermal conduction could affect these results, a calculation has been made with the initial reflected shock velocity one-half the ideal frozen value. In this manner the maximum initial effect of thermal conduction on the inviscid flow is included.[13] The resulting end-wall pressure variation is shown on Fig. 7, and it is qualitatively identical to the radiative cooled case. Thus, in comparison to radiative cooling, shock velocity variations resulting from thermal conduction have only a small effect on the end-wall pressure behavior.

Since some investigators[14] have used end-wall pressure measurements to determine chemical reaction rates, these results are very important because they indicate that the prediction and interpretation of wall pressure results behind strong reflected shock waves should include the effects of radiative transfer. In addition, if such a pressure dip can be detected experimentally, it offers a new yet straightforward method of studying radiative-gasdynamic coupling phenomena.

In the present analysis the flowfield properties behind the incident shock wave are assumed to be constant. In actuality, however, incident shock gas ingested by the reflected shock front is variable due to chemical relaxation in the incident zone; and this variation may affect the above results. Consequently, a nonequilibrium chemistry normal shock computation has been carried out for the 11 km/sec, 10 μ Hg incident shock wave. The results indicate that for the time period considered in the present calculations the gas in front of the reflected shock wave corresponds to the tail of the incident shock relaxation zone and that the flow properties in this region vary only 6–8%. Nevertheless, even such small gradients can affect the reflected shock flowfield. For example, using the approximate analysis of Ref. 15 a 6% increase in the density in the incident region will induce a 5% increase in the pressure behind the reflected shock wave. This change, however, is small compared to the 50% decrease due to radiative cooling that is shown on Fig. 7. Thus, it is believed that the effects of gradients due to incident shock relaxation upon the reflected shock flowfield is small when compared to the effects of radiative cooling.

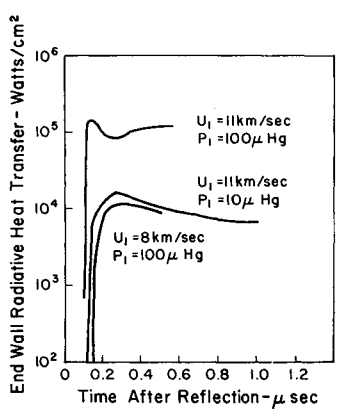

Fig. 9 End-wall radiative heat transfer behind reflected shock waves.

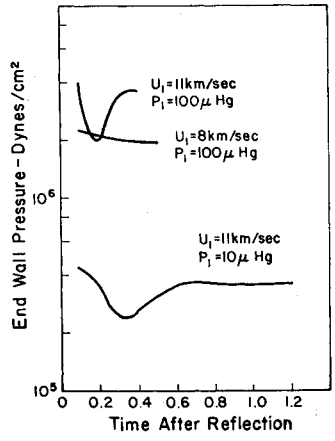

Fig. 10 End-wall pressure variations behind reflected shock waves.

Table 2 End-wall radiative heat transfer 0.4 μsec after reflection

Incident shock speed, km/sec	Initial pressure mm Hg	Region two	Radiative cooling included	qR 620–1570 Å kw/cm²	qR 1570–9552 Å kw/cm²
11	0.01	Equilibrium	Yes	11.75	0.25
11	0.01	Equilibrium	No	43.23	2.00
11	0.01	Frozen	Yes	8.27	0.16
11	0.10	Equilibrium	Yes	108.30	1.63
8	0.10	Equilibrium	Yes	10.56	0.37

On the other hand, the actual magnitude of species concentrations in the incident zone may be more important than gradients since these magnitudes affect both chemical relaxation and radiative rates. Consequently, a comparison calculation has been carried out which conservatively assumes incident properties corresponding to the start of the tail of the incident relaxation zone. At this point the amount of ionization is comparatively small and the density is only 71% of the equilibrium value. Hence, the results of this calculation should indicate the maximum effect due to small initial species concentrations.

All of the results obtained are qualitatively identical in features and trends to those portrayed in Figs. 2–7, and typical profiles are presented in Fig. 8. As can be seen, the end-wall pressure still exhibits the strong 50% initial decrease due to radiative cooling. The actual minimum value does, however, occur slightly later, indicating a slight retardation in cooling due to the low initial concentrations. Comparison of the temperature and velocity profiles of Fig. 8 with those of Figs. 5 and 6 shows that in this case the relaxation zone is longer. Still, as evidenced by the velocity acceleration towards the wall and the different electron and heavy particle temperatures, there is strong radiative-gasdynamic coupling and extensive thermal nonequilibrium. Based upon these comparisons, it is concluded that while incident shock species concentration values quantitatively affect the reflected shock flowfield they do not qualitatively change the effects of radiative cooling or thermal nonequilibrium presented above.

One of the major purposes of this investigation has been to examine the effects of chemical and thermal nonequilibrium on the end-wall radiative heat transfer. The results for three incident shock velocity initial pressure combinations are shown on Fig. 9. Since the radiative transfer processes are related to the electron temperature, the radiative heat transfer should reflect any large variations in the electron temperature; and Fig. 9 shows this to be the case. Initially, when the electron temperature is only slightly higher than its preshock value, the radiative heat transfer is negligible. However, the heat transfer for all three cases increases very rapidly and achieves a temporary maximum value at a time that in each case corresponds almost exactly to the peak electron temperature (i.e., Fig. 2). From this correspondence it is concluded that during the initial period after reflection the end-wall radiative heat transfer varies in the same manner as the electron temperature.

After the peak the total heat transfer decreases, and as shown by the 11 km/sec-100 μ Hg results, eventually begins to slowly increase. This phenomena is due to the existence of two competing effects. First, during this time period the electron temperature is steadily decreasing, thus reducing the amount of energy being radiated by a given element of gas. Second, the slug of radiating gas is steadily increasing in size since the shock is moving away from the end-wall. Since the gas is practically transparent, almost all radiative energy emitted in the direction of the wall will reach the wall. Consequently, it is possible, even with a decreasing electron temperature, for the radiative heat transfer to increase with time simply because of the increased number of radiating particles.

The spectral composition of the end-wall radiative heat transfer at 0.4 μsec after reflection is listed in Table 2. As can be seen, the contribution from the vacuum-ultraviolet-continuum and vacuum-ultraviolet-lines (620–1570 Å) in each case exceeds by about two orders of magnitude that due to the visible continuum and infrared lines (1570–9552 Å). This dominance of the vacuum-ultraviolet region is characteristic of low density flows and is in contrast to analytic[1] and experimental[2] results at higher pressures (i.e., 1.0 mm Hg), where the visible continuum usually dominates.

To ascertain whether or not two temperature and cooling effects are important, additional calculations of the end-wall radiative heat transfer for the 11 km/sec-10 μ Hg case have been made with 1) no radiative cooling and 2) with the electron temperature equal to the heavy particle temperature. In the first case the result at 0.7 μsec was about 6×10^4 w/cm² while in the second it was an unrealistically large 10^{10} w/cm². For comparison, the complete calculation predicts 8×10^3 w/cm². Thus, these results indicate that thermal nonequilibrium and radiative cooling must be explicity accounted for in the calculation of end-wall radiative heat transfer at short times.

In order to determine at least approximately the effects of incident shock velocity and initial pressure on the above results, two additional calculations corresponding to 11 km/sec and 8 km/sec incident shock velocities and an initial pressure of 100 μ Hg have been carried out. Figure 10 compares the end-wall pressure variation for the three cases, and it can be seen that the pressure decrease due to radiative cooling also occurs in the higher pressure 11 km/sec-100 μ Hg case. However, at the 8 km/sec condition there is no evidence of the radiative-transfer-pressure interaction. Since radiative effects are strongly dependent upon shock velocity, this result is not too surprising; but it does serve to indicate that the magnitude of the radiation is a primary factor in determining whether or not the pressure-radiative transfer interaction occurs. The initial pressure appears to only affect how rapidly it occurs.

Figure 11 portrays a similar comparison of the temperature profiles in the reflected shock region. Here all three cases are similar in that the relaxation regions are all characterized by extensive thermal nonequilibrium. Furthermore, in each case the electron temperature approaches the heavy body temperature from below; and, in fact, examination of the

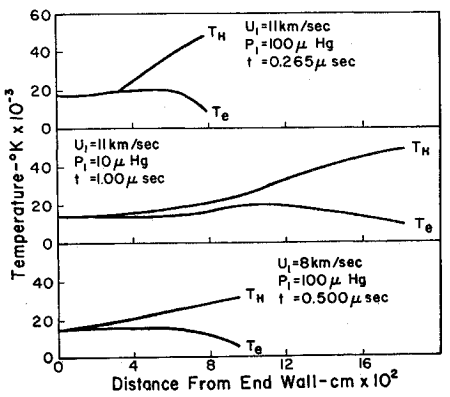

Fig. 11 Comparison of temperature profiles behind reflected shock waves.

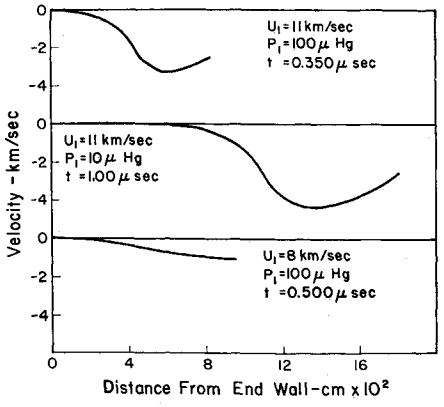

Fig. 12 Comparison of velocity profiles behind reflected shock waves.

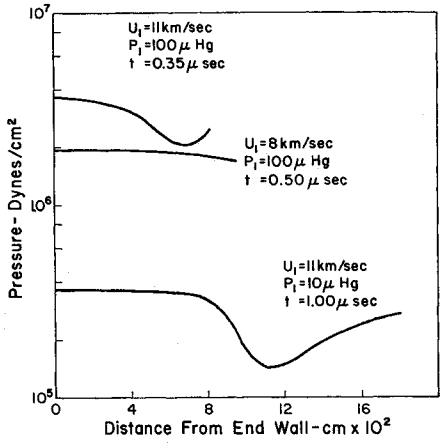

Fig. 13 Pressure profiles behind reflected shock waves.

calculations indicates that even in the local equilibrium region the electron temperature is always about 2% below the heavy particle temperature. This result is particularly significant since several investigators[16,17] have recently measured reflected shock temperature and obtained values that are usually slightly lower than those predicted by shock velocity gasdynamic relationships. Possibly, based upon the present computations and the fact that these investigators primarily used spectroscopic techniques, the explanation for the difference is that the measured values are electron temperatures and the gasdynamically predicted values are heavy particle temperatures. Furthermore, these two temperatures reach pseudo-equilibration rather quickly but do not attain complete equilibration for some time.

Representative velocity profiles are shown for the three cases on Fig. 12. As in the end-wall pressure case the two 11 km/sec conditions evidence extensive radiative-gasdynamic coupling in that there is a velocity acceleration towards the wall, but the 8 km/sec results display a more usual velocity profile. Again the magnitude of the radiation appears to be the dominating factor in determining whether or not radiative-gasdynamic coupling occurs.

Additional evidence of the possibility of strong radiation coupling in the relaxation zone is presented in Fig. 13, which presents typical pressure profiles for the three cases considered. These profiles bear a strong resemblance to the end-wall profiles in Fig. 10, and both 11 km/sec cases show a relaxation zone pressure decrease due to radiative cooling.

These results demonstrate that for the conditions of the present investigation radiative-gasdynamic coupling and two-temperature effects exist and are important in the reflected shock flowfield for short times after reflection. The results also indicate that if these effects are ignored, completely erroneous trends may be obtained for the pressure, velocity, and temperature variations.

Conclusions

The following general conclusions can be drawn from the present study of the effects of chemical and thermal nonequilibrium in the flowfield behind a reflected shock wave in nitrogen.

1) At short times after reflection a major portion of the reflected shock flowfield exhibits a high degree of chemical and thermal nonequilibrium. These nonequilibrium effects exert a strong influence on the nature and character of the flowfield behind the reflected shock wave. If accurate results are desired, their effects cannot be neglected.

2) Immediately behind a reflected shock wave in nitrogen the important ionization process is atom-atom collisions. However, as soon as the number of electrons becomes significant and the electron temperature increases, electron-atom collisions become the dominant ionization mechanism. The atom-ion reaction is always relatively unimportant.

3) Initially in the reflected shock flowfield the effects of radiative cooling and collision exchange can be sufficient to cause the end-wall pressure to decrease significantly. Only after thermal equilibration does the end-wall pressure exhibit the pressure rise usually associated with chemical relaxation.

4) Radiative-gasdynamic coupling can have a pronounced effect on the pressure and velocity profiles in the relaxation region behind the reflected shock front. In fact, completely erroneous velocity and pressure profiles may be obtained if radiative transfer is omitted from the energy equation.

5) Two temperature effects must be explicitly included in order to obtain correct radiative-gasdynamic coupling results and to predict accurate end-wall radiative heat-transfer rates.

References

[1] Anderson, J. D., Jr., "Radiative Transfer Effects on the Flowfield and Heat Transfer Behind a Reflected Shock Wave in Air," *The Physics of Fluids*, Vol. 10, No. 8, Aug. 1967, pp. 1785–1793.

[2] Golobic, R. A. and Nerem, R. M., "Shock Tube Measurements of End-Wall Radiative Heat Transfer in Air," *AIAA Journal*, Vol. 6, No. 9, Sept. 1968, pp. 1741–1747.

[3] Nerem, R. M., Carlson, L. A., and Hartsel, J. E., "Chemical Relaxation Phenomena Behind Normal Shock Waves in a Dissociated Freestream," *AIAA Journal*, Vol. 5, No. 5, May 1967, pp. 910–916.

[4] Chapin, C. E., "Nonequilibrium Radiation and Ionization in Shock Waves," AA&ES 67-9, June 1967, Purdue Univ., Lafayette, Ind.

[5] Oettinger, P. E. and Bershader, D., "A Unified Treatment of the Relaxation Phenomena in Radiating Argon Plasma Flows," *AIAA Journal*, Vol. 5, No. 9, Sept. 1967, pp. 1625–1632.

[6] Carlson, L. A., "Expressions for the Exchange of Energy and Momentum Between Gases at Different Temperatures and Velocities," *The Physics of Fluids*, Vol. 13, No. 7, July 1970, pp. 1869–1870.

[7] Wilson, J., "Ionization Rate of Air Behind High Speed Shock Waves," *The Physics of Fluids*, Vol. 9, No. 10, Oct. 1966, pp. 1913–1921.

[8] Knott, P. R., Carlson, L. A., and Nerem, R. M., "A Further Note on Shock Tube Measurements of End-Wall Radiative Heat Transfer in Air," *AIAA Journal*, Vol. 7, No. 11, Nov. 1969, pp. 2170–2172.

[9] Carlson, L. A., "Radiative Transfer, Chemical Nonequilibrium, and Two-Temperature Effects Behind a Reflected Shock Wave in Nitrogen," Ph.D. dissertation, 1969, The Ohio State Univ., Columbus, Ohio.

[10] Nerem, R. M. and Stickford, G. H., "Shock Tube Studies of Equilibrium Radiation," *AIAA Journal*, Vol. 3, No. 6, June 1965, pp. 1011–1018.

[11] Zel'dovich, Y. B. and Raizer, Y. P., *Physics of Shock Waves and High-Temperature Hydrodynamic Phenomena*, Vol. II, Academic Press, New York, 1966, p. 506.

[12] Petschek, H. and Byron, S., "Approach to Equilibrium Ionization Behind Strong Shock Waves in Argon," *Anals of Physics*, Vol. 1, 1957, pp. 270–315.

[13] Hay, G. D., "An Approximate Small-Time Solution for a Transparent Radiating Gas Behind a Reflected Shock Wave," M. Sc. thesis, 1968, The Ohio State Univ., Columbus, Ohio.

[14] Hanson, R. K., "An Experimental and Analytical Investigation of Shock Wave Reflection in a Chemically Relaxing Gas," SUDAR 345, May 1968, Stanford Univ., Stanford, Calif.

[15] Hanson, R. K. and Baganoff, D., "Reflection of a Shock Wave into a Density Gradient," *AIAA Journal*, Vol. 8, No. 4, April 1970, pp. 805–807.

[16] Wood, A. D. and Wilson, K. H., "Radiant Energy Transfer Measurements in Air," CR-1390, Oct. 1969, NASA.

[17] Bengtson, R. et al., "Comparison of Measured and Predicted Conditions Behind a Reflected Shock," *The Physics of Fluids*, Vol. 13, No. 2, Feb. 1970, pp. 372–377.

MAY 1971 AIAA JOURNAL VOL. 9, NO. 5

Thermal Modeling of the Human Body—Further Solutions of the Steady-State Heat Equation

JOHN C. CHATO* AND AVRAHAM SHITZER†
University of Illinois at Urbana-Champaign, Urbana, Ill.

The thermal behavior of the human body has been modeled with particular emphasis on direct cooling of the skin by cooling tubes used in current extravehicular activity (EVA) space units. Steady-state analytical solutions have been obtained for several boundary conditions and for various values of the parameters involved. Although the results provide insight into the problem and even compare acceptably with some of the scant previous investigations, much more work is needed both analytically and, especially, experimentally before the numerical results can be considered reliable for biological purposes. The analysis presented herein is, nevertheless, applicable to any steady-state heat conduction problem in rectangular bodies with internal heat generation.

Nomenclature‡

a = half-distance between cooling tubes (L)
A = total skin surface area (L^2)
b,b_1,b_2 = depth of tissue (L)
F,F_1 = uniform heat flux [$q/(t - L^2)$]
$f(x)$ = variable heat flux [$q/(t - L^2)$]
f_a = average heat flux, defined by Eq. (7), [$q/(t - L^2)$]
f_1,f_2 = constant heat flux, at $x = 0$ and $x = \beta a$, respectively, [$q/(t - L^2)$]
k,k_1,k_2 = thermal conductivity [$q/(t - L - T)$]
n = summation integer
Q = defined by Eq. (2), (T/L^2)
Q_0,Q_1,Q_2 = internal heat generation rate per unit volume [$q/(t - L^3)$]
T = tissue temperature (T)
T_1,T_2* = constant temperature at inner core (T)
T_{ref} = reference temperature (T)
x = direction normal to cooling strips along skin surface (L)
y,y_1,y_2 = direction normal to skin surface (L)
α_n = coefficient in a Fourier series, defined by Eq. (8), [$q/(t - L)$]
β = fraction of skin cooled
λ_n = separation coefficient, defined by Eq. (6), (L^{-1})
ξ = integration variable (L)
ϕ = defined by Eq. (4), (T)

Received May 11, 1970; revision received September 14, 1970. This work was supported in part by NASA Grant NGR 14-005-103. B. A. Hertig, Director of the Laboratory for Ergonomics Research of the University of Illinois at Urbana-Champaign, gave considerable help on the physiological aspects of the problem. The manuscript was prepared by the able staff of the Publications Office of the Department of Mechanical and Industrial Engineering. The numerical calculations were performed in the Digital Computer Laboratory of the University.

* Professor of Mechanical Engineering, Department of Mechanical and Industrial Engineering. Member AIAA.

† Research Assistant, Department of Mechanical and Industrial Engineering.

‡ The units in parentheses are L = length, p = force, q = heat (P-L), t = time, T = temperature.

Introduction

ALTHOUGH the thermal behavior of a biological system such as the human body is very involved, it becomes necessary in certain engineering applications to establish a model that can simulate at least certain major aspects of the heat transfer within the living tissues. Our interest in these phenomena arose from the problems of developing advanced thermoregulatory systems for protective suits to be used in hostile environments, such as outer space. These thermoregulatory systems must remove the metabolic heat generated by the body and they must compensate for all external heat effects under all conditions encountered.[1] The most recent Apollo space suits achieved metabolic heat removal by a network of water-cooled tubes in direct contact with the skin. Buchberg and Harrah[2] applied a numerical method to a steady-state model which represented the human body as a set of rectangular strips. The width of these strips was the mean half-distance between cooling tubes. The depth was divided into four layers: an outer layer of skin, a so-called functional periphery, a musculature, and an essentially constant temperature inner core. The tissues were considered isotropic. Thermal conductivity and internal heat generation were considered functions of temperature and were adjusted to compensate for the effects of blood flow.

The purpose of our analytical investigations was to obtain steady-state solutions for a similar model which, however, does not require numerical solutions. To achieve this goal, the thermal properties and the internal heat generation rate were taken as constants; and the two "working" layers of